Extension of the Johnson-Mehl-Avrami-Kolmogorov theory incorporating anisotropic growth studied by Monte Carlo simulations

Kooi, BJ

Published in:
Physical Review. B: Condensed Matter and Materials Physics

DOI:
10.1103/PhysRevB.73.054103

Publication date:
2006

Extension of the Johnson-Mehl-Avrami-Kolmogorov theory incorporating anisotropic growth studied by Monte Carlo simulations

B. J. Kooi*
Department of Applied Physics, Materials Science Centre and Netherlands Institute for Metals Research, University of Groningen, Nijenborgh 4, 9747 AG Groningen, The Netherlands
(Received 24 August 2005; revised manuscript received 16 November 2005; published 7 February 2006)

An analytical theory has been developed, based on Monte Carlo (MC) simulations, describing the kinetics of isothermal phase transformations proceeding by nucleation and subsequent growth for d-1 dimensional growth in d dimensional space (with d 2 or 3). This type of growth is of interest since it is generally anisotropic, leads to hard impingement, and obtains strong deviations from the traditional Johnson-Mehl-Avrami-Kolmogorov (JMAK) theory. Within the MC simulations 1D growth can occur with equal probability in two or three different nonparallel orientations in 2D space. In 3D space 2D growth can occur with equal probability in three (or two) different orthogonal orientations. The MC simulations show that initially always a regime is present where JMAK theory prevails, but that after a well-defined critical time a transition to a blocking regime occurs. Both regimes are characterized by clearly different, but nearly constant values of the Avrami exponent which depend on the dimensionality of growth and space and on the time dependence of nucleation. The dependence of the critical time and of the extended fraction within the blocking regime (based on the concept of the extended volume of the JMAK theory) on the nucleation and growth parameters has been extensively analyzed and all results of the MC simulations have been captured within the analytical theory.

DOI: 10.1103/PhysRevB.73.054103 PACS number(s): 81.30.Hd, 68.55.Ac, 02.70.Uu

I. INTRODUCTION

The fraction transformed as a function of time for the isothermal phase transformation proceeding via nucleation and subsequent growth is generally described by the Johnson-Mehl-Avrami-Kolmogorov (JMAK) theory.[1–3] Several conditions have to be fulfilled before JMAK kinetics will hold and therefore under practical conditions deviations from JMAK kinetics, although sometimes small, are more the rule than the exception. Often it is stated that JMAK kinetics require isotropic growth, but this is not a necessary condition. Growth can be anisotropic as long as the transformation products (grains) have convex shape and the orientation of the anisotropy axes of all grains are aligned parallel (so that for each direction in transformation space all grains have identical growth velocity, where the velocity may vary with the direction in space).[4,5] When the growth rate in certain directions in transformation space differs for various grains, i.e., nontrivial cases of anisotropic growth, then the JMAK theory is not valid anymore and clear deviations occur (defined as a nonconstant Avrami exponent as a function of time). A proper analytical theory in the spirit of the JMAK theory that accounts for anisotropic growth has not been developed. Attempts into this direction were made by Birnie III and Weinberg,[6,7] but predominantly for one-dimensional (1D) space; in 2D space only pre-existing nuclei were assumed (i.e., site saturation) and the possibility that grains grow around each other was excluded. Another option is, of course, to extend the mathematical formulation of the JMAK theory, adding (one or more) new variables that provide freedom to improve the agreement in case anisotropic growth occurs.[8–11] However, the aim of the present work is to derive an analytical description that is theory based and not phenomenological, i.e., where all variables have physical meaning.

In order to develop and test such a theory, Monte Carlo (MC) or similar types of simulations are powerful, because in this way ideal experiments can be mimicked, where the nucleation and (anisotropic) growth processes are well known and controlled, but nevertheless occur in a natural manner. This type of ideal experiments in conjunction with JMAK theory have, of course, been performed to quite some extent; see, e.g., the Refs. 4, 5, and 12–14. In some cases the simulations were performed to confirm the JMAK theory,[4,5,11–13] in some cases to show (numerical) deviations from the JMAK theory,[4,5,14] but only rarely was the analytical JMAK theory extended in order to account for the (numerical) deviations provided by the simulations. A nice example of this last case can be found in Ref. 14, where during the transformation two phases develop simultaneously (with variable space fractions), where each phase shows isotropic growth, but where the growth rate of the two phases can differ. In a one-dimensional space the faster growing phase cannot grow around the slower one and increasing deviations from the mean-field (JMAK) result occur for increasing difference in growth speeds. As shown in Ref. 14 these deviations almost completely vanish when going to two-dimensional space. Extrapolating on this result means that in this particular case the JMAK theory is accurate in 3D space.

In the present work results of Monte Carlo simulations in both 2D and 3D space are presented, and in all cases the deviations from JMAK kinetics due to anisotropic growth are large. MC simulations of nucleation and growth in 3D space have previously been reported in Ref. 13, but were restricted to isotropic growth. The most advanced MC simulations of anisotropic growth were presented by Pusztai and Granasy, but hold for 2D space.[5] In their simulations mutual blocking of growing grains, that were allowed to grow around each other, occurred up to all relevant orders. Their

simulations provided numerical results that clearly showed the deviations from JMAK kinetics, but unfortunately did not improve our understanding of the underlying physical problem than already available *a priori*. The main purpose of the present work is the development of an analytical theory that can describe the (numerical) deviations from JMAK theory as provided by MC simulations. Moreover, it will show the first MC simulations of nucleation and anisotropic growth in 3D space.

Only linear growth is considered (i.e., the growth rate is independent of time) that, e.g., holds for interface controlled (diffusion-less) transformations, for instance, encountered during crystallization of amorphous phases. It has to be remarked that the growth modes adopted in the present work are kept relatively simple (see Sec. III, where the growth modes shown in Fig. 4 are explained). For instance, in 3D space, growth of square plates based on three possible orthogonal orientations is considered. The advantage of the growth modes adopted is that they do not lead to approximations (can be treated exactly) and thus lead to reliable and accurate results. Moreover, these growth modes can occur in nature, for instance, when nucleation and growth occur on {100} planes of a cubic parent phase. Although 1D growth in 2D space is analyzed predominantly to improve theoretical understanding, this type of growth can actually occur in thin films. All the anisotropic growth considered leads to blocking effects that retard the transformation process compared to the isotropic case. Interfacial-energy effects that, for instance, during coalescence of the transformation, products can accelerate the transformation process which are neglected within the present work. For isotropic growth it has been shown that such effects of surface tension are important.[15] For anisotropic growth the importance is definitely less, because the contact area between coalescing grains, e.g., thin orthogonal plates, is relatively much smaller.

The number of independent growth directions that are considered in the present work is limited to three. Hence, the general problem of randomly oriented anisotropic growth as treated in Ref. 5 is not addressed. There are two reasons for this limiting choice: (1) Transformation of a crystalline parent phase, where growth of the new phase is anisotropic, generally occurs in specific crystalline directions of the parent phase; in this sense consideration of a limited number of growth directions is of more practical importance, because encountered more frequently in nature than the general problem mentioned above. (2) It turned out possible to derive the analytical theory that reproduces the transformation kinetics based on these limited growth directions and to find interesting scaling phenomena, but this turned out not yet possible for the general problem. Nevertheless, the present paper extends substantially on our previous paper[16] (i) by performing MC simulations in 2D space where the orientation for growth is not necessarily orthogonal, but can have an arbitrary angle and (ii) by performing MC simulations in 3D space. All the results of the MC simulations are captured in a single analytical equation [Eq. (8) below] that in the limit incorporates the JMAK theory fully, but also describes the deviations due to anisotropic growth as a function of the nucleation and growth rates (and other physical parameters) in both 2D and 3D space.

II. THEORETICAL BACKGROUND

The kinetics of isothermal phase transformation proceeding via nucleation and subsequent growth are generally described by the JMAK theory that states that the fraction of transformed space x is related to the extended fraction x_{ex} according to[3–7,13,16]

$$x(t) = 1 - \exp[-x_{ex}(t)], \tag{1a}$$

where the extended fraction obeys

$$x_{ex} = \int_0^t I(\tau) V(t-\tau) d\tau, \tag{1b}$$

with I the nucleation rate per unit of untransformed space and V the extended space of a single transformation product (hereafter called grain) at time t when it was nucleated at time τ. Equation (1) only holds for an infinite transformation space where nucleation has equal probability to occur anywhere in space and with an extended space V of the grains having either an isotropic or anisotropic shape, but in the latter case the shape has to be convex and the orientation (of the anisotropy axes) of all grains has to be parallel.[4,16]

If the growth rate G, for a given temperature, is constant in time and if the total number of nuclei formed per unit of untransformed space with dimension d_s, for a given temperature, is a simple power of time t according to $N=N_0 t^a$ ($a \geqslant 0$), then it can be easily derived that Eq. (1b) becomes

$$x_{ex} = g \prod_{i=1}^{d_g} \left(\frac{i}{i+a} \right) N_0 G^{d_g} t^{d_g + a} \tag{2}$$

with d_g the dimensionality of growth and g a geometrical constant depending on the shape of the grains (e.g., for a spherical grain $g=4\pi/3$ and for a square plate with thickness w $g=4w$). The extended fraction thus depends on the time to the power d_g+a where this power is generally called the Avrami exponent or the transformation index n. The prefactor before the time dependence in Eq. (2) is often taken as the variable k and then Eqs. (1a) and (2) boil down to a format often used for the JMAK theory:

$$x(t) = 1 - \exp(-kt^n). \tag{3}$$

In the remainder of the paper the Avrami exponent is defined as the local slope in the so-called Avrami plot $\ln[-\ln(1-x)]$ versus $\ln(t)$. Then a nonconstant Avrami exponent as a function of time can be considered a deviation from normal JMAK behavior.

Equation (2) shows that the dimensionality of growth can be different (equal or lower) than the dimensionality of space. However, if the dimensionality of growth is lower, JMAK behavior in Eq. (1) is only valid if the orientation of the growing grains is parallel. If this is not the case, blocking of growing grains occurs which leads to strong deviations from JMAK behavior. Attempts to extend the JMAK theory to incorporate this type of blocking were made which generally assumed that Eq. (1a) had to be modified.[8–11] However, in a previous paper[16] we showed, based on Monte Carlo simulations, that for one-dimensional growth in two-dimensional space, where grains grow with equal probability

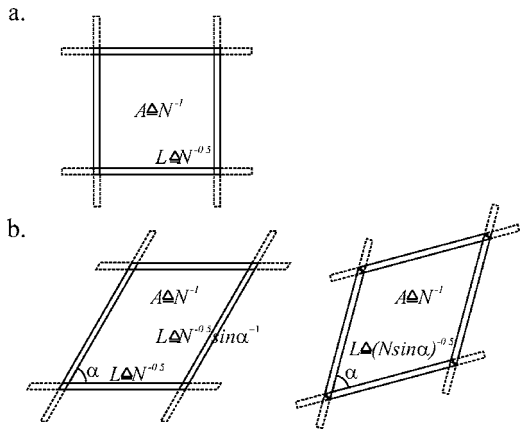

FIG. 1. Schematic representation of the average length L 1D grains (with width w) are able to grow in 2D space before blocking occurs, when the total number of nuclei per unit of area present is N. (a) Growth has equal probability of occurring in two orthogonal orientations. (b) Growth has equal probability of occurring in two orientations making a mutual angle α.

in two orthogonal orientations, it is more correct to modify Eq. (1b). Also Birnie III and Weinberg derived analytical equations for anisotropic growth in 1D and 2D space (with random orientation of particles, in 2D space only accounting for site saturation, i.e. pre-existing nuclei, without the possibility that grains grow around each other) where Eq. (1b) was modified and not Eq. (1a).[6,7] In the present paper it will be shown, again based on Monte Carlo simulations, that the modification of Eq. (1b) remains valid if 1D growth has equal probability to occur in any two or three arbitrary orientations in 2D space and for 2D orthogonal growth in 3D space.

For 1D growth in 2D space, where grains grow with equal probability in two orthogonal orientations, we showed[16] based on MC simulations that, after an initial period where normal JMAK behavior is valid, a blocking regime is entered where $V(t-\tau)$ in Eq. (1b) has to be replaced by the width w times the average length the grains are able to grow before blocking occurs:

$$V(t-\tau) = \frac{wC}{\sqrt{N_0 \tau^a}}, \tag{4}$$

where C turned out to be a constant with a value close to 2. It is important to note that the average length the grains are able to grow before blocking occurs, and thus Eq. (4), is independent of the growth rate G. The validity of Eq. (4) can be rationalized on the basis of the average length 1D grains are able to grow with orthogonal orientation in 2D space; this length is directly related to the average distance between the grains and this average distance in 2D space is the reciprocal of the square root of the total number of nuclei at time t; see the graphical representation in Fig. 1(a). In Fig. 1 A denotes the area per nuclei, L the length that the nuclei are able to grow before blocking occurs, and N the total number of nuclei and/or grains present per unit area. Note explicitly that this total number of nuclei includes the so-called phantom nuclei in the same way as they are included in the extended volume in the traditional JMAK theory;[3,17–19] only in the case of pre-existing nuclei, $a=0$, phantom nuclei do not occur. Phantom nuclei are finally properly accounted for when going from the extended fraction to the actual fraction transformed in Eq. (1a). Using this knowledge Eq. (1b) becomes

$$x_{ex} = \int_{t^*}^{t} a N_0 \tau^{a-1} \frac{wC}{\sqrt{N_0 \tau^a}} d\tau \tag{5a}$$

with t^* given by

$$G t^* = \frac{C}{\sqrt{N_0 (t^*)^a}} \Rightarrow t^* = \sqrt[a+2]{\frac{C^2}{N_0 G^2}}. \tag{5b}$$

Integration of Eq. (5a) yields

$$x_{ex} = 2wC\sqrt{N_0 (t-t^*)^a}, \tag{6}$$

where up to t^* the extended fraction obeys normal JMAK behavior according to Eq. (2) and after t^* the blocking regime is entered and the total extended fraction is thus given by the sum of the fractions pertaining to the JMAK and the blocking regime:

$$x_{ex} = 2wC\sqrt{N_0 (t-t^*)^a} + \left(\frac{2w}{1+a}\right) N_0 G (t^*)^{1+a}. \tag{7}$$

As will be shown later by MC simulations and here also by basic reasoning it turns out that this approach can be readily extended to 1D growth in 2D space where the two directions do not have to be orthogonal. In case the angle between the two orientations is α, then the only modification needed is that the constant C in the above equations has to be divided by $\sqrt{\sin\alpha}$. This result can be understood by noting that, for the same area defined by the average distance between the nuclei as in the orthogonal case, the edges now can be $(\sin\alpha)^{-1/2}$ times longer; see Fig. 1(b). (Of course note that the final result is a statistical average of many local blocking events with various mutual positions of nuclei that interact after growth and therefore the schematic cases shown in Fig. 1(b) on the left and right side lead finally to the same average result.) It is important to note that for parallel ($\alpha=0°$) growth of grains with anisotropic (convex) shape the division of C by $\sqrt{\sin\alpha}$ leads to a t^* in Eq. (5b), which becomes infinite and thus the normal JMAK theory [Eq. (2)] then fully holds. Also in case, not two, but three different orientations are possible in which 1D growth can occur with equal probability. The above equations can be used directly. For instance, if the mutual angles between the three orientations is 60°, then the area enclosed is $\frac{1}{2}\sqrt{3}$ of the orthogonal case (with two orientations) but with $\frac{3}{4}$ of the number of 1D grains. Hence, the constant C has to be multiplied by $\sqrt{(1/2\sqrt{3})/(3/4)}$. However, an extension to the general case, where growth can occur in any random orientation, is not directly possible within the present approach and is also not the purpose of the present work.

On the other hand, the extension of these results for 1D growth in 2D space to 2D growth in 3D space is again readily possible and is provided in the Appendix.

According to this previous analysis the total extended fraction is described as the sum of the fractions holding for the JMAK and blocking regime, cf. Eqs. (7) and (A4). This excellently reproduces the overall MC simulations (for orthogonal 1D growth in 2D space) as shown in Fig. 2. However, Fig. 2(c) shows that the transition from the JMAK behavior to the blocking regime is modeled poorly (as was already explained in our previous paper[16]). In Fig. 3 results are shown, where growth in the 2D space has equal probability to occur in three different orientations, namely two orthogonal and one making 45° with these orthogonal orientations. The different curves hold for different constant nucleation rates ($a=1$ with respect to a constant growth rate G; for the parameters used in the MC simulations see Table I). From Fig. 3(c) it is clear that the various curves show identical behaviors apart from a scaling factor t^*, that is the critical time denoting the transition from the JMAK to the blocking regime. Both regimes are characterized by a (more or less) constant level of the Avrami exponent. In the JMAK regime the Avrami exponent is d_g+a and in the blocking regime it approaches a/d_s. Also in Fig. 3(b) accurate scaling behavior can be observed regarding the levels of the straight-line segments in the Avrami plot. A kinetic description, that accounts for the two level states and the gradual transition between them [as shown in Fig. 3(c) and the actual positions of the straight lines as shown in Fig. 3(b)], that is based on all MC simulations performed for 1D growth in 2D space and 2D growth in 3D space as will be explained in more detail below in Sec. IV, can be derived to have the following form:

$$x_{ex} = \frac{kt^n}{\left[t^p + (t^*)^p\right]^{(n-m)/p}}, \tag{8a}$$

$$n = d_g + a, \tag{8b}$$

$$m = a/d_s, \tag{8c}$$

$$k = wK^{d_g}\sqrt[d_s]{N_0}, \tag{8d}$$

$$t^* = \sqrt[1+m]{\frac{K}{\left[\frac{g}{w}\prod_{i=1}^{d_g}\left(\frac{i}{i+a}\right)\right]^{1/d_g}\sqrt[d_s]{N_0}G}}, \tag{8e}$$

where K is a kind of universal constant with a value near 2.95. Note that if $t \ll t^*$ Eq. (8) boils down exactly to the normal JMAK equation Eq. (2) and if $t \gg t^*$ Eq. (8) becomes

$$x_{ex} = wK^{d_g}\sqrt[d_s]{N_0}t^m \tag{9}$$

that is nearly identical to Eq. (6) (for $d_g=1$ and $d_s=2$) and Eq. (A3) (for $d_g=2$ and $d_s=3$). Similarly, Eq. (8e) shows clear resemblance with Eq. (5b) (for $d_g=1$ and $d_s=2$) and Eq. (A2b) (for $d_g=2$ and $d_s=3$). Note that t^* is now defined as the time when the Avrami exponent obtains a value exactly in-between the two constant levels pertaining to the JMAK and the blocking regime, i.e., $(n+m)/2$. This time t^* is now slightly longer than as based on the definitions given in Eqs. (5b) and (A2b) (cf. Fig. 2) and therefore K is somewhat larger than C. Equation (8) leads to a single master curve if the time t is scaled with respect to t^* and the extended fraction x_{ex} with respect to $k(t^*)^m$ (cf. Fig. 3).

The main advantage of Eq. (8) is that it is able to model the gradual transition from the JMAK to the blocking regime quite well, but the price is that a parameter p has been added (that has less physical basis than all other parameters) that quantifies the transition rate. In principle, p accounts for the fact that not only the average length grains are able to grow before blocking occurs is important, like used in Eqs. (4) and (A1), but also the size distribution around this average length. The MC simulations show that for fixed values of n and m, p is a constant independent of the nucleation factor N_0, the growth rate G, the width w, and the mutual angle between the growing grains.

Note that the remarks made above, with respect to the modification of the constant C in case grains, are not growing orthogonal orientations in 2D space; but with a mutual angle α, or that three instead of two growth orientations are active, are identically valid for the constant K in Eq. (8). In fact, Eq. (8) turns out to be better in reproducing or the MC simulations for the various angles α than Eq. (7). Equation (8) nearly exactly reproduces *all* behavior shown in Fig. 3. Therefore in Fig. 3 the theoretical fits cannot be distinguished from the curves based on the MC *simulations*! In some other cases the MC simulations show behavior that slightly deviates from Eq. (8); these instances will be highlighted below within Sec. IV, but overall Eq. (8) turns out to be very powerful in predicting the complete transformation kinetics of d-1 dimensional growth in d-dimensional space. Its main limitation is that it assumes that, when the Avrami exponent is plotted as a function of logarithm of time [cf. Fig. 3(c)], the transition rate from the JMAK exponent n to the blocking exponent m is exactly symmetrically around t^* $[(n+m)/2]$, but in general the transition occurs faster from n to t^* than from t^* to m.

As treated in our previous paper,[16] also the thickening of the d-1 grains (a constant increase of w in time with a rate lower than the nominal growth rate G of the d-1 grains) can be incorporated in the present theory. Hence, the present theory extends the applicability of the traditional JMAK theory substantially in a natural and transparent manner and as will be shown in Sec. IV, this analytical theory is strongly supported and firmly based on MC simulations.

III. COMPUTATIONAL PROCEDURE

The Monte-Carlo simulations performed in the present work are based on similar procedures as adopted in our previous work,[16] but extended to (2D growth in) 3D space. The isothermal transformation was analyzed in 2D and 3D space, allowing nucleation and growth to occur in a typical area of 1000 by 1000 pixels in 2D space and volumes of $200 \times 200 \times 200$ pixels (voxels) in 3D space, where in all cases periodic boundary conditions were applied. To test the possible size effects areas of 2000×2000 pixels and volumes of $400 \times 400 \times 400$ voxels were also used. Basically, individual MC runs (providing, e.g., the fraction transformed x as a function of time t for certain nucleation and growth param-

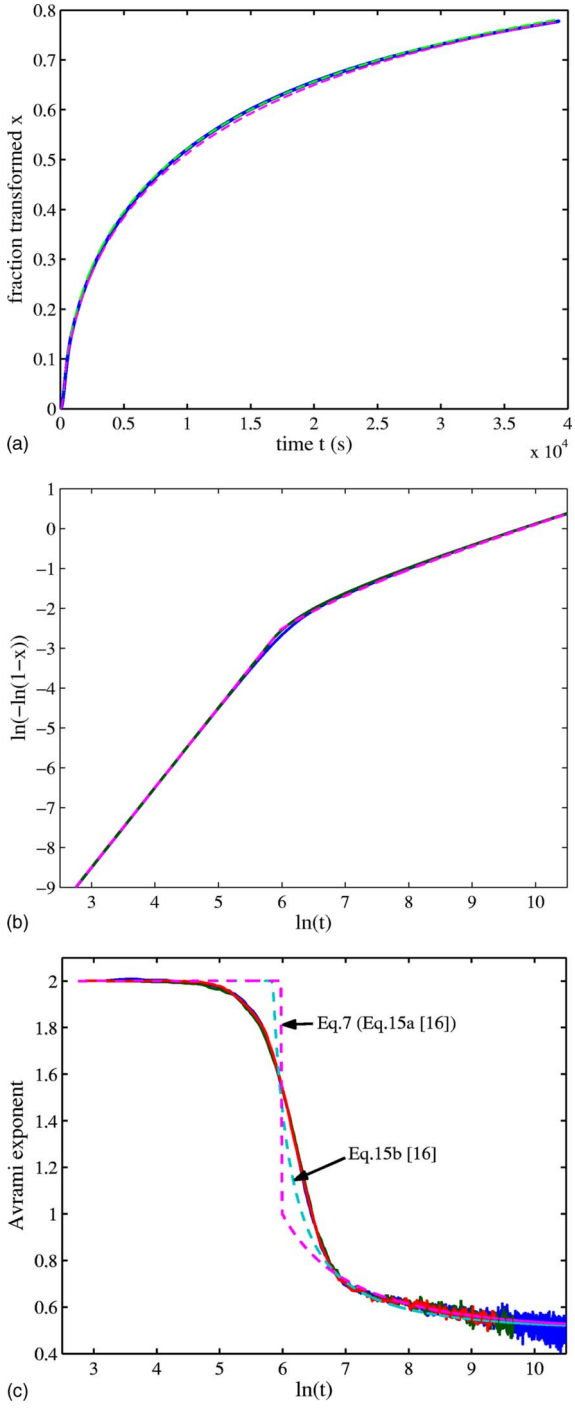

FIG. 2. (Color online) Transformation kinetics obtained by MC simulations as based on continuous nucleation and 1D orthogonal growth in 2D space (solid lines) together with theoretical predictions based on Eq. (7) of the present paper (Eq. 15a in our previous paper[16]) and on Eq. 15b in our previous paper[16] (dashed lines). In (a) the fraction transformed x is plotted as a function of time t, (b) shows the Avrami plot, i.e., $\ln[-\ln(1-x)]$ versus $\ln(t)$, and in (c) the Avrami exponent as derived from the slope in (b) is plotted versus $\ln(t)$. The theoretical predictions (without the fitting parameter) excellently reproduce the MC simulations; only Fig. 1(c) shows that the transition from the JMAK regime to the blocking regime is not reproduced properly by theory. The parameters used for the MC simulations are given in Table I.

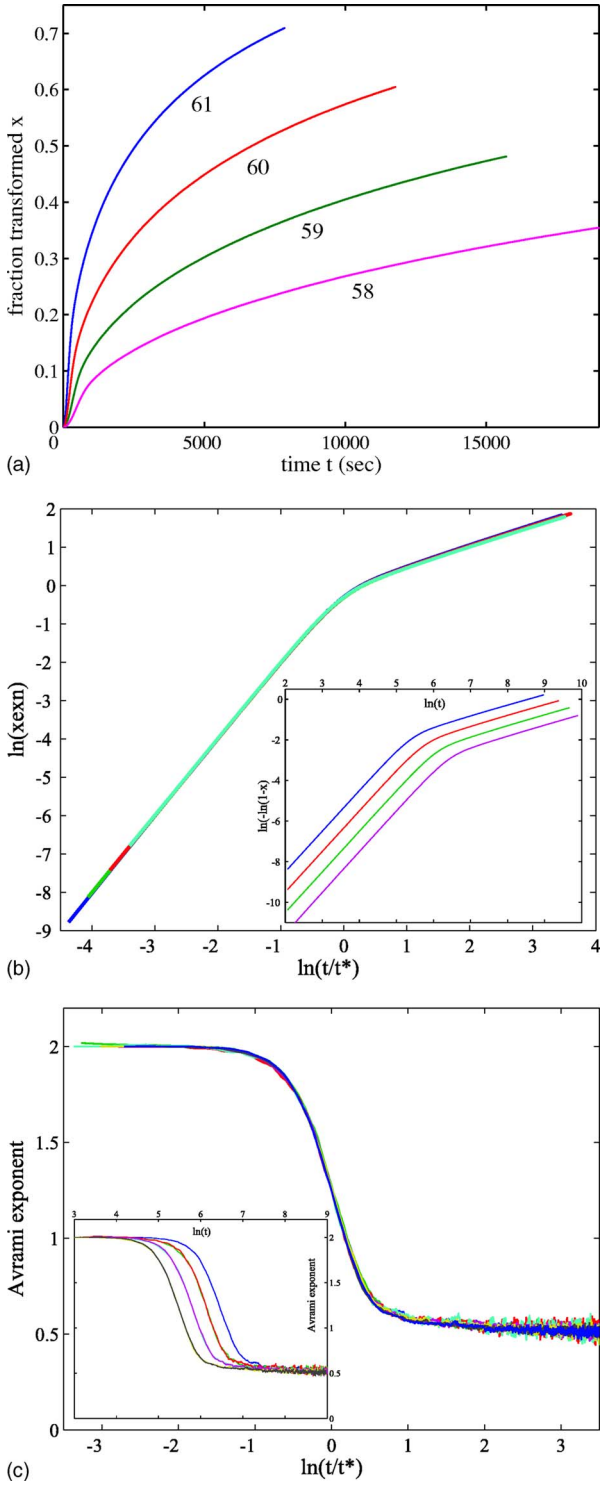

FIG. 3. (Color online) Results of MC simulations where 1D growth in 2D space had equal probability of occurring in three different orientations: two orthogonal ones and one making 45° with these other two. The parameters used for the MC simulations are given in Table I. In (a) the fraction transformed x is plotted as a function of time t. (b) shows the Avrami plot, i.e. $\ln[-\ln(1-x)]$ versus $\ln(t)$, as the inset in the fully scaled figure with $\ln(xexn) = \ln([-\ln(1-x)]/k(t^*)^m)$ along the y axis and $\ln(t/t^*)$ along the x axis; see Eq. (8). (c) shows the Avrami exponent as derived from the slope in Fig. 2(b) versus $\ln(t/t^*)$ and versus $\ln(t)$ in the inset.

TABLE I. Parameters used for the Monte-Carlo simulations whose results are shown in the various figures indicated. The total number of nuclei per unit of area is described by Eq. (10) and the growth rate by Eq. (12); also all of the symbols used are defined.

	System Size	Pixel Size (μm)	Temperature T (K)	a	$\ln(N_0)$	E_n (eV)	G_0 (μm/s)	E_g (eV)
Fig. 2	1000^2	0.01	373	1	59 $\mu m^{-2} s^{-1}$	2.0	exp(40)	1.5
Fig. 3	1000^2	0.01	373	1	58, 59, 60, and 61 $\mu m^{-2} s^{-1}$	2.0	exp(40)	1.5
Fig. 5	1000^2	0.01	373	1	61 $\mu m^{-2} s^{-1}$	2.0	exp(40)	1.5
Fig. 6	1000^2	0.01	373	1	Varied (58–62) $\mu m^{-2} s^{-1}$	2.0	exp(40)	1.5
Fig. 7	1000^2	0.01	373	0	17, 18, 19, and 20 μm^{-2}	0.5	exp(40)	1.5
Fig. 8	1000^2	0.01	373	0	Varied (16–20.5) μm^{-2}	0.5	exp(40)	1.5
Fig. 9	200^3	0.05	373	1	57 $\mu m^{-3} s^{-1}$	2.0	exp(40)	1.5
Fig. 10	400^3	0.025	373	1	57, 58, 59, and 60 $\mu m^{-3} s^{-1}$	2.0	exp(40)	1.5
Fig. 11	200^3	0.05	373	1	Varied (55–58) $\mu m^{-3} s^{-1}$	2.0	exp(40)	1.5
Fig. 12	200^3	0.05	373	0	13, 14, 15, and 16 μm^{-3}	0.5	exp(40)	1.5
Fig. 13	200^3	0.05	373	0	Varied (13–16) μm^{-3}	0.5	exp(40)	1.5

eters) show larger statistical variations for a smaller sized system. However, the average results of many MC runs appeared, as tested several times in our work for the nucleation and growth parameters used, not to depend on the two sizes indicated above for both 2D and 3D space. The systems are self-averaging and although the underlying processes are stochastic in nature the systems as a whole behave deterministically.[15]

Nucleation. The number of nuclei per unit of untransformed space N as a function of time t and temperature T is expressed as[16,20,21]

$$N(t,T) = N_0 t^a \exp\left(\frac{-E_n}{k_B T}\right) \tag{10}$$

with E_n the activation energy for nucleation and k_B Boltzmann's constant and N_0 a constant independent of time and temperature. Nucleation occurs for certain values of a, N_0, and E_n and T. In each time step Δt, the number of newly appearing nuclei is defined by the nucleation rate derived from Eq. (10) multiplied by Δt. Each nucleus is assigned to a pixel with position p,q by using a random number generator (RNG) to obtain the p and the q values independently. The pixel p,q is not assigned to a position that is already transformed by nucleation and growth in the previous time steps and the use of the RNG is *repeated* until a position within the untransformed space is assigned. This directly implies that Eq. (10) is defined per unit of untransformed space and thus, for each next time step the total space has to be multiplied by $(1-x)$, as obtained in the previous time step. Using this method, so-called phantom nuclei[3,16,18,19] are not an issue. In order to maximize accuracy, the number of nuclei that form within the time step i, NR_i, is described by the following recursive procedure, where A is the actual area or volume considered in the simulations:

$$NR_i = floor\left(\sum_{j=1}^{i} N_j A(1-x_{j-1})\right) - \sum_{j=1}^{i-1} NR_j, \tag{11}$$

with

$$N_j = aN_0(j\Delta t - \Delta t/2)^{a-1} \exp\left(\frac{-E_n}{k_B T}\right)\Delta t,$$

where floor means rounding to the lower integer number. Note that Eq. (11) is only valid for $a>0$. The situation of pre-existing nuclei, $a=0$, is of course easily implemented within the MC simulations. The present treatment of nucleation leads, as we tested, to less statistical fluctuations than the more simple and straightforward procedure adopted by Pusztai and Granasy.[5] Their assumption that nucleation always occurs instantaneously at the beginning of a time step is not accurate for time-dependent nucleation; e.g., for a constant nucleation rate (in combination with a constant growth rate) it is better to assume that nucleation occurs in the middle of the time step.

Growth. The growth rate G is described by a simple Arrhenian temperature dependence:

$$G(T) = G_0 \exp\left(\frac{-E_g}{k_B T}\right) \tag{12}$$

with E_g the activation energy for growth (>0) and G_0 a constant independent of time and temperature; i.e., only linear growth is considered. The time step Δt is chosen such that within one time step the growth rate G times Δt exactly corresponds to the size of one pixel (e.g., for a total area of 10 by 10 μm represented by 1000 by 1000 pixels the pixel size is 10 nm). Various growth models were adopted for the present work. Usually isotropic spherical (circular) growth and/or anisotropic elliptical growth are assumed. Since both total area and pixel are, in general, square, the sphere or ellipse has to be approximated. This may introduce additional errors or at least makes the calculations (unnecessary) more demanding since the pixel size has to be small to allow accurate approximation of these curved shapes. Moreover, the results must, in principle, be obtained for various pixel sizes and then extrapolated to an infinite small pixel size. To circumvent these uncertainties, a different approach is taken in the present work. Four different growth modes as sche-

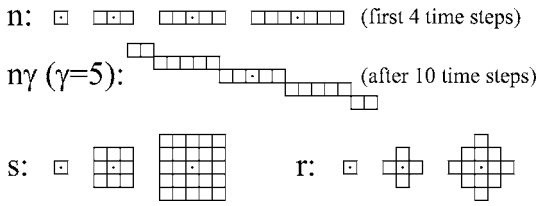

FIG. 4. Schematic representation of the various growth modes adopted in the present work. The ***n*** and ***nγ*** modes are used in 2D space and the ***s*** and ***r*** modes in 3D space. The ***nγ*** growth mode is shown only for $\gamma=5$ after ten time steps. A random number generator can be used to assign the grains to have one of two orthogonal orientations in 2D space and one of three orthogonal orientations in 3D space. The ***nγ*** mode is always used in combination with a single orientation of the ***n*** mode in order to mimic the situation where growth has equal probability of occurring in two orientations with mutual angle α.

matically depicted in Fig. 4 have been considered: one-dimensional ***n*** (needle) and ***nγ*** growth in two-dimensional space and 2D ***s*** (square) and ***r*** (rectangular) growth in 3D space. If the growth occurs with all grains oriented parallel, normal JMAK behavior results. More interesting behavior is observed if the orientations are not parallel. For the ***n*** growth mode a RNG is used to assign the growth of a certain nucleus and/or grain with equal probability to either one of the two orthogonal orientations. The ***nγ*** growth mode is always defined in combination with a single orientation of the ***n*** growth mode such that the γ value denotes the number of pixels that the grains of ***nγ*** and ***n*** are parallel before the ***nγ*** grain makes a step in a direction perpendicular to the growth direction of ***n***. Also in this case a RNG is used to assign nucleated grains to have either the ***n*** or ***nγ*** growth mode. Note that for all the cases of 1D growth in 2D space the grain on each side advances each time step with one pixel. For the ***s*** and ***r*** growth modes a RNG is used to assign a certain nucleus and/or grain with equal probability to either one of three orthogonal directions (also results will be shown where the growth occurs only in one or two of the possible three orthogonal orientations). The results presented in Sec. IV (and in our previous work[15]) show that these simple growth modes provide clear and extensive conclusions on deviations from JMAK kinetics due to impingement, allowing the development of the analytical theory, e.g., as summarized in Eq. (8). Note that (2D) circular growth is intermediate between the ***s*** and the ***r*** growth modes adopted here.

As a matter of course, the growth of each grain during each time step proceeds such that it is checked, for each pixel that by the growth mode is allowed to become part of the growing grain, if it is already assigned to another grain that arrived earlier at the pixel. Only if it is not already assigned, it becomes part of the growing grain. Note that impingement is taken into account up to all relevant orders as explained in Refs. 4 and 5 and that it is allowed that grains grow around each other, but a new pixel must remain connected to a previously incorporated pixel in the grain. However, this last point "growing around" is impossible for 1D growth in 2D space. This makes the computational procedure very simple. The growth (advancement with one pixel) on each side of the original pixel that was the nucleus can proceed each time step after nucleation until a pixel is reached that is already transformed. Then growth on this side ceases and is not considered for this grain on this side in this and the remaining time steps. For 2D growth in 3D space, grains can definitely grow around each other. This type of growth is treated exactly by allowing growth around a pixel in time step *i only* if it was transformed in time step *i*-1. With the ***r*** growth mode only the four nearest neighbors of such a pixel are considered for the next growth step, whereas with the ***s*** growth mode the eight nearest neighbors of such a pixel are considered (cf. Fig. 4). In principle, this means that only the outer pixels at the circumference of each grain are able to grow, but not the outer pixels that reached the circumference earlier than the last time step. This is important in order to prevent that grains with different growth speeds in a certain direction are able to cross each other (where the fast-growing one can overtake within the simulations the slower growing one without actually growing around this slower grain), instead of the natural process where grains can impinge and then may grow around each other. So, although relative simple growth shapes are assumed the growth itself occurs in a complete natural manner.

IV. RESULTS AND DISCUSSION

A. 1D growth in 2D space with continuous nucleation

The transformation kinetics in 2D space of the ***n*-*nγ*** growth mode (cf. Fig. 4) for various values of γ (0, 1, 3, 5, 19) are shown in Fig. 5. The other parameters used for the MC simulations in this example are given in Table I. A γ value 0 indicates that growth is orthogonal and with increasing γ value the two orientations in which 1D growth can occur become increasingly parallel (cf. Fig. 4). In Figs. 2(b) and 2(c) it can be seen that the kinetics can be divided into two regimes; the initial regime follows normal JMAK behavior with an Avrami exponent 2 as expected for continuous nucleation ($a=1$) and 1D growth. Also as expected, in this regime the result does not depend on the mutual orientation of the grains with anisotropic shape, i.e., γ value [cf. inset in Fig. 5(b)]. Then a transition to the blocking regime occurs, where the Avrami exponent has a value near to $\frac{1}{2}$. According to the theory in Sec. II it should approach the value $\frac{1}{2}$ exactly (as was the case in Figs. 2 and 3 and in our previous work[15]). However, now for increasing γ value it tends to approach systematic lower values, although the statistical fluctuations also strongly increase, because the fraction transformed approaches a value 1 and then the discreteness of the MC simulations causes limitations. The main effect of γ is that the transition (time) to the blocking regime occurs later for increasing γ value. In fact for parallel growth the transition time becomes infinite and only the JMAK regime occurs.

The influence of the γ value on blocking can be understood as follows. The density of ***n*** grains, growing say in the *x* direction, determines on average their mutual distance in the *y* direction and this is the same for all simulations in Fig. 5. Blocking of the ***nγ*** grains thus occurs if they have grown the same number of pixels in the *y* direction. This means that for $\gamma \geqslant 1$ the ***nγ*** grains can grow γ times longer (in time and

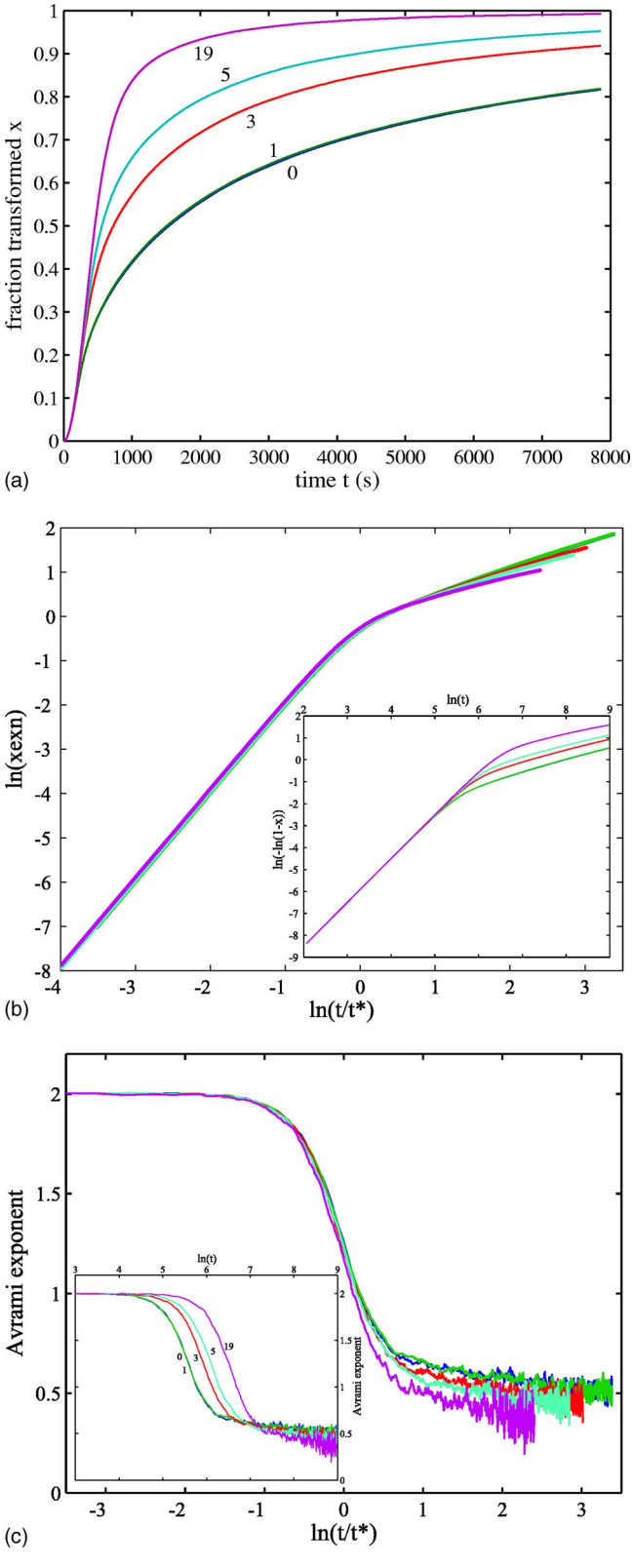

FIG. 5. (Color online) Same three figure types as used for Fig. 3, but now showing the results of MC simulations where 1D growth in 2D space had equal probability to occur in two different orientations as defined by the $\boldsymbol{n}$ and $\boldsymbol{n\gamma}$ modes in Fig. 4 for various values of $\boldsymbol{\gamma}$ (0, 1, 3, 5, 19). The parameters used for the MC simulations are given in Table I.

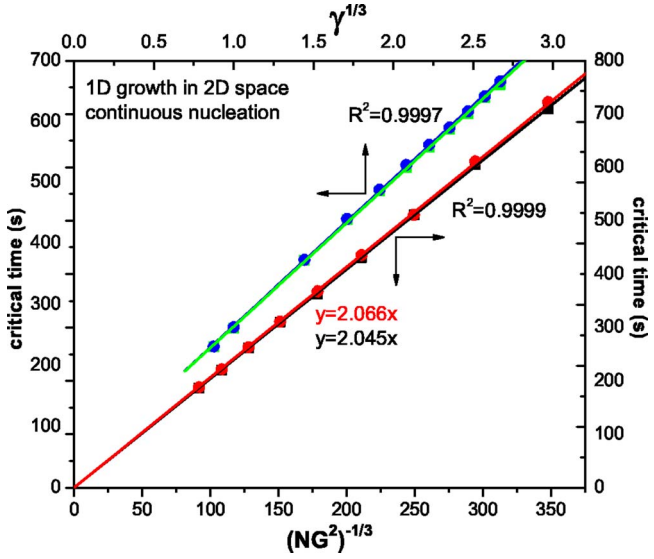

FIG. 6. (Color online) Results that hold for a constant nucleation rate and 1D growth in 2D space and that are based on the average of 21 MC simulations. The critical time t^* is plotted as a function of $\boldsymbol{\gamma}^{1/3}$ using the top and left axes (for increasing $\boldsymbol{\gamma}$ values the $\boldsymbol{n\gamma}$ and $\boldsymbol{n}$ grains become increasingly parallel; cf. Fig. 4). A more or less linear relation appears to exist. The critical time t^* is plotted as a function of $(NG^2)^{-1/3}$ using the bottom and right axis, showing that t^* is directly proportional to $(NG^2)^{-1/3}$; see Eq. (8).

length) than in the orthogonal case before blocking occurs, because the growth mode allows per growth front an average advance in the y direction per time step of $1/\boldsymbol{\gamma}$ pixel (and 1 pixel in the x direction). For $(0\leqslant)\boldsymbol{\gamma}\leqslant 1$, all results are identical as for orthogonal growth, because each time step the growth front is allowed to advance 1 pixel in the y direction (and on average $\boldsymbol{\gamma}$ pixel in the x direction). The $\boldsymbol{\gamma}$ value has no influence on the blocking of the $\boldsymbol{n}$ grains. The final result is that, statistically, the average length all grains (both $\boldsymbol{n}$ and $\boldsymbol{n\gamma}$) can grow before blocking occurs in 2D space is $\sqrt{\boldsymbol{\gamma}}$ longer than for the orthogonal case for $\boldsymbol{\gamma}\geqslant 1$. In this discrete situation (with pixels) the $\boldsymbol{\gamma}$ value has exactly the same meaning as $1/\sin\alpha$ in the continuum situation explained in Sec. II and Fig. 1. (When using $\boldsymbol{\gamma}$ in the sense of $1/\sin\alpha$ the identical results obtained for $0\leqslant\boldsymbol{\gamma}\leqslant 1$ should actually be considered to have originated from a $\boldsymbol{\gamma}$ value 1.)

According to Eq. (8) the transition time t^* for $d_g=1$, $d_s=2$ and $a=1$ (and thus holds when the Avrami exponent obtains a value 1.25) is directly proportional to $K^{2/3}$ and K itself is proportional to $1/\sqrt{\sin\alpha}$, so that t^* is proportional to $(\sin\alpha)^{-1/3}$. For the present simulations it means that t^* is a linear function of $\boldsymbol{\gamma}^{1/3}$. In Fig. 6 this relation is plotted using the left and top axes and is based on the data provided by the MC simulations for the same parameters as used for Fig. 5. Indeed, it can be seen that this relation accurately holds (but is not exact). Note that for each $\boldsymbol{\gamma}$ value an average of 21 MC simulations was used to obtain, on the basis of the standard deviation, an upper and lower bound for the time needed to reach an Avrami exponent of 1.25. Also note that the result of growth in three different orientations in 2D space (two orthogonal ones and the third making 45° with the other two) as shown in Fig. 3 is incorporated in Fig. 6. In this case the

area enclosed is $\frac{1}{2}$ of the purely orthogonal case but with $\frac{3}{4}$ of the number of 1D grains and thus the γ value is $\frac{1}{2}/\frac{3}{4}=\frac{2}{3}$ which fits well within the trend provided by the other data shown in Fig. 6 and later in Fig. 8.

In Fig. 6 another linear relation is plotted using the bottom and right axes, but now N_0 is varied [between exp(58) and exp(62) μm^{-2} s^{-1}] for a constant value of $\gamma=0$ (orthogonal growth) and the other parameters identical as for Fig. 5. Figure 6 shows that the critical time t^* is directly proportional to $(NG^2)^{-1/3}$; this relation is exact. According to Eq. (8) the slope in Fig. 6 is equal to $K^{2/3}$ and thus Fig. 6 indicates, as based again on the average of 21 MC runs, a K value in-between 2.92 and 2.97. Very similar values for K will be found in the next three sections (Secs. III B–III D), showing the universality of Eq. (8).

Results for a nucleation rate that increases linearly in time (meaning that the total number of nuclei is a quadratic function of time), i.e., $a=2$, show that the Avrami exponent has a value of 3 in the JMAK regime and a minimum value of 1 in the blocking regime. Because of space limitations not all these results are shown. However, it is interesting to state here that a linear relation is found between t^* and $(NG^2)^{-1/2}$, and that the slope indicates a K-value of 2.88.

B. 1D growth in 2D space of pre-existing nuclei

Non parallel 1D growth in 2D space based on pre-existing nuclei leads to transformation kinetics where an initial JMAK regime exists characterized by an Avrami exponent with a value of exactly 1 followed by a gradual transition to a value of 0 in the blocking regime. An example of this behavior is shown in Fig. 7 using parameters for the MC simulations that are given in Table I. The transition to an Avrami exponent 0 means that the transformation stops before being complete and thus the fraction transformed reaches an upper limit x_{max} below one. As can be seen in Fig. 7 interesting scaling behavior occurs regarding the value of x_{max}. In fact as predicted by Eq. (8) for scaling not x_{max} itself but the extended fraction $-\ln(1-x_{max})$ has to be considered and should be directly proportional to the square root of N_0, because for $t \gg t^*$: $x_{ex}=k=wK^{d_g}\sqrt[d_s]{N_0}$. Indeed, as shown in Fig. 8, using the bottom and right axes, this relation holds exactly and the slope in Fig. 8 indicates a K value of 2.96 (because $w=0.01$ μm). Note, as explicitly tested, that x_{max} is not (significantly) depending on the growth rate G. In Fig. 8 the extended fractions $-\ln(1-x_{max})$ as obtained by the MC simulations for various values of γ are plotted as a function of $\sqrt{\gamma}$ using the top and left axes. Again the relation is directly proportional and thus in accordance with Eq. (8). Based
on this latter relation a K value of 2.92 holds. Note that each value of x_{max} used in Fig. 8 (and the corresponding hardly visible error bar) is based on the average of 21 MC simulations.

C. 2D growth in 3D space with continuous nucleation

Two types of 2D growth modes are considered in 3D space as explained in Sec. III and shown in Fig. 4, the

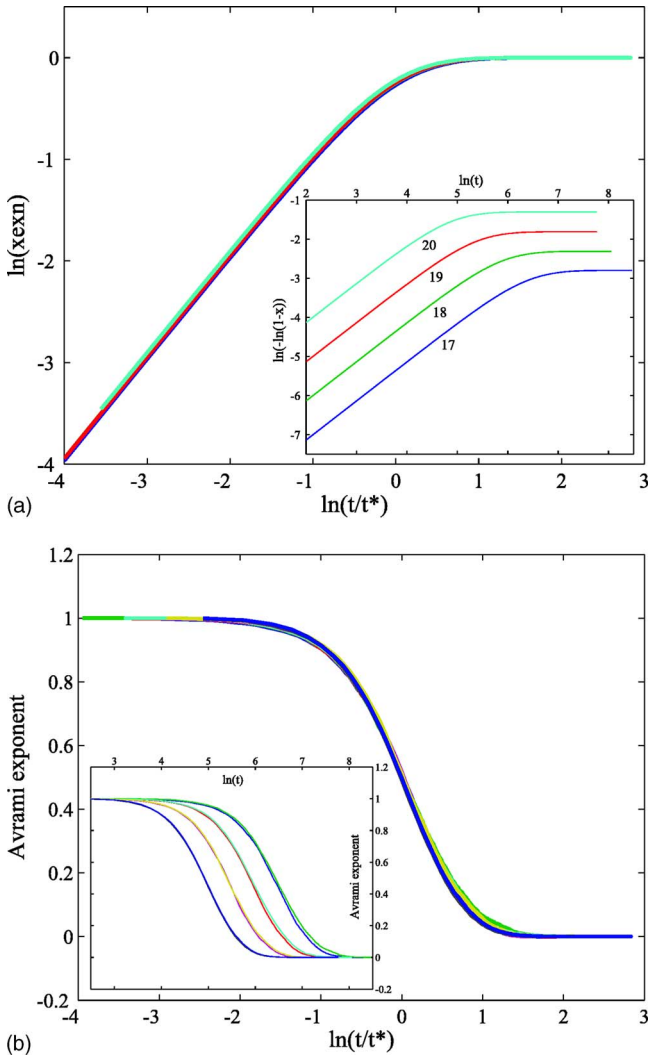

FIG. 7. (Color online) Transformation kinetics obtained by averaging 21 MC simulations for 1D orthogonal growth in 2D space as based on pre-existing nuclei. (a) The Avrami plot, i.e. $\ln[-\ln(1-x)]$ versus $\ln(t)$ with x the fraction transformed and t the time in the inset of the fully scaled figure with $\ln(xexn)=\ln[-\ln(1-x)/k(t^*)^m]$ along the y axis and $\ln(t/t^*)$ along the x axis; see Eq. (8). (c) shows the Avrami exponent as derived from the slope in Fig. 7(a) versus $\ln(t/t^*)$ and versus $\ln(t)$ in the inset. The parameters used for the MC simulations are given in Table I.

s(quare) and ***r***(ectangular) modes. If all ***s*** or ***r*** grains grow parallel only JMAK behavior is expected and this is indeed observable in Fig. 9. The example shown in Fig. 9 holds for MC simulation parameters given in Table I. As expected according to JMAK theory for 2D growth and continuous nucleation ($a=1$), parallel growth yields a constant Avrami exponent with a value of 3 for almost the entire x (fraction transformed) interval from 0 to 1 [see s and r lines in Fig. 9(b)]. Note that for $x>0.9$ the Avrami exponent starts to deviate from the value 3 due to the limited resolution of the MC simulations (relative small number of untransformed pixels remain) and the sensitivity of the Avrami exponent.

Compared to parallel growth, strong blocking is observed if the ***s*** and ***r*** grains have equal probability to grow in three orthogonal orientations; see curves indicated $s3$ and $r3$ in

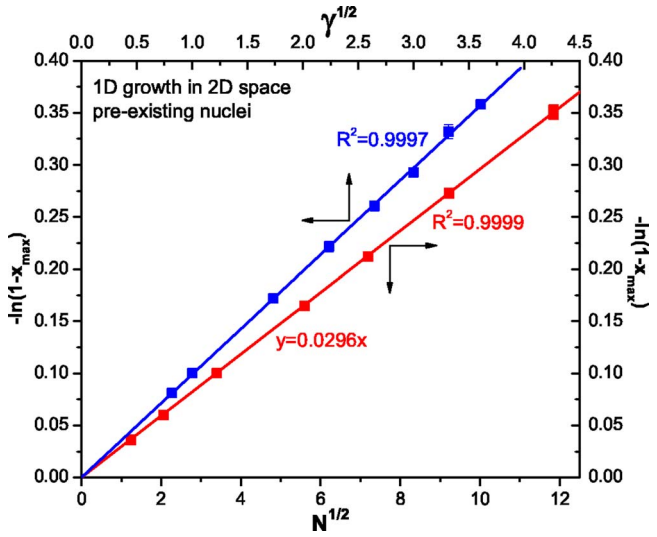

FIG. 8. (Color online) Results that hold for pre-existing nuclei and 1D growth in 2D space and that are based on the average of 21 MC simulations. The extended fraction based on the maximum attainable fraction transformed is plotted (using the right axis) versus the square root of the total number of pre-existing nuclei per unit of area N (using the bottom axis); grains grow with equal probability in two orthogonal orientations. The same extended fraction is plotted (using the left axis) versus the square root of $\boldsymbol{\gamma}$ (using the top axis) (for increasing $\boldsymbol{\gamma}$ values the $\boldsymbol{n\gamma}$ and $\boldsymbol{n}$ grains become increasingly parallel; cf. Fig. 4).

Fig. 9. It is important to note that, as expected for the JMAK regime, the initial difference in transformation rate for the $s3$ and $r3$ growth vanished in the blocking regime [see Fig. 9(a)]. The mutual orientation of the plates in space control the blocking regime, but the shape (and as shown in Sec. IV B and in Ref. 16 also the rate G) with which the individual grains can grow become irrelevant in the blocking regime. Figure 9(c) again clearly indicates that these two (JMAK and blocking) regimes are present. Note that the Avrami exponents of the $\boldsymbol{s}$ and $\boldsymbol{r}$ modes are initially not equal to 3. However, it is clear that the circular growth that is intermediate between $\boldsymbol{s}$ and $\boldsymbol{r}$ growth will have an Avrami exponent that is 3. According to Eqs. (10)–(12) an Avrami exponent of $\frac{1}{3}$ is expected within the blocking regime. Indeed this value approximately holds within this regime, but in fact is approached from lower values relatively long after the transition from the JMAK to the blocking regime has occurred. Although it is difficult to prove, it is likely that the slowly increasing value of the Avrami exponent observed within the blocking regime is related to the "growth around" that is possible. For 1D growth in 2D space only pure blocking can occur, whereas now the plates can definitely grow around each other.

For completeness also results are shown where the $\boldsymbol{s}$ and $\boldsymbol{r}$ grains have equal probability to grow in two (out of the three) orthogonal orientations (see $s2$ and $r2$ curves in Fig. 9); then say in the x and y direction strong blocking occurs, but in the z direction growth is parallel and in this direction normal JMAK impingement occurs. The $s2$ and $r2$ curves indeed show intermediate behavior between the parallel growth and the growth in the three orthogonal orientations.

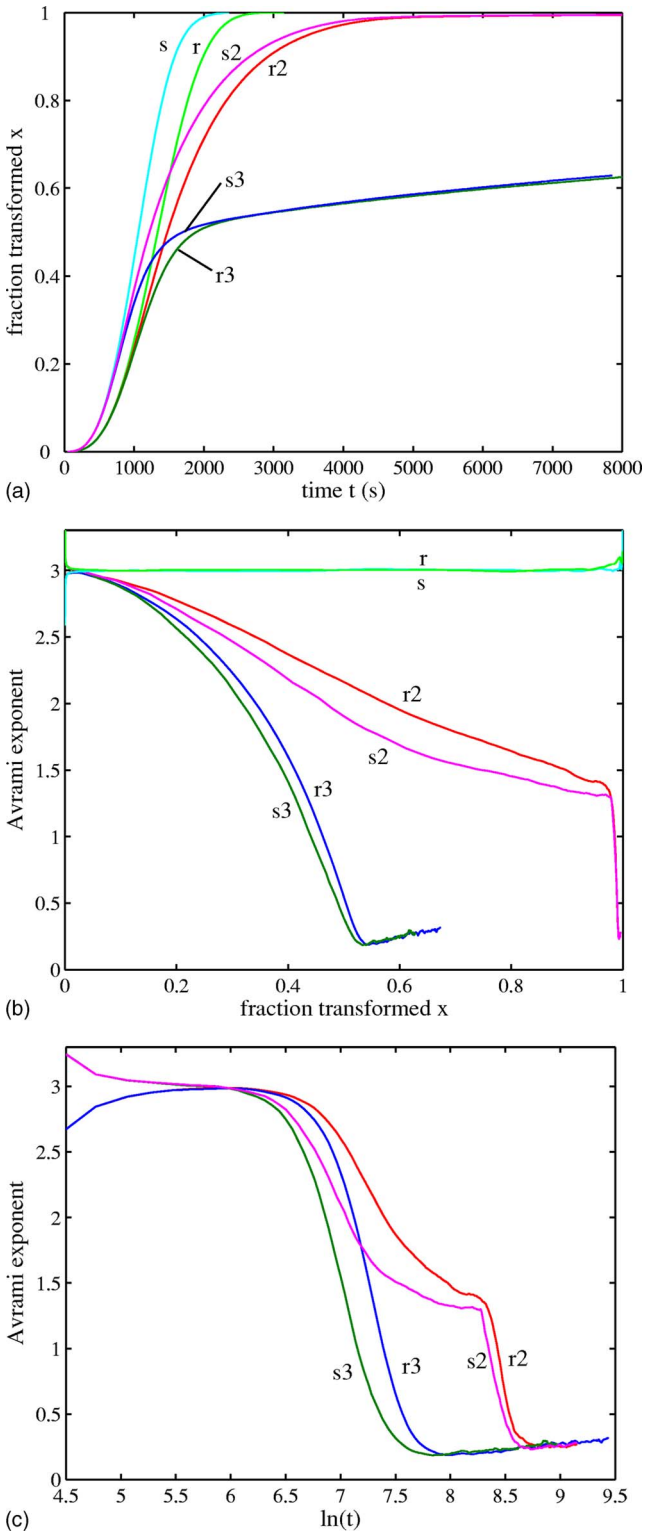

FIG. 9. (Color online) Transformation kinetics obtained from MC simulations based on a constant nucleation rate and 2D $\boldsymbol{s}$ and $\boldsymbol{r}$ growth in 3D space (cf. Fig. 4). The $\boldsymbol{s}$ and $\boldsymbol{r}$ grains grow parallel, i.e., grow all in one out of three possible orthogonal orientations (denoted as s and r), grow with equal probability in two (out of the three) possible orthogonal orientations (denoted as $s2$ and $r2$) and grow with equal probability in three orthogonal orientations (denoted as $s3$ and $r3$). The parameters used for the MC simulations are given in Table I.

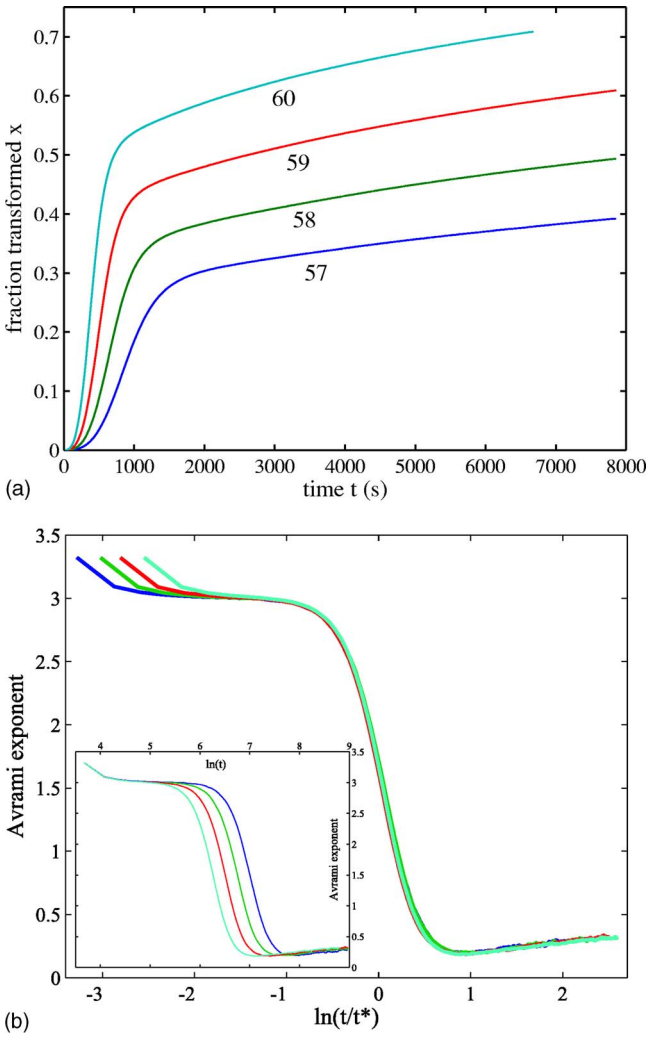

FIG. 10. (Color online) Transformation kinetics obtained from MC simulations based on a constant nucleation rate and 2D *s* growth in 3D space containing 64 million voxels. The *s* grains grow with equal probability in three orthogonal orientations. The parameters used for the MC simulations are given in Table I.

According to Fig. 9(b) no apparent relation between $s2/r2$ and $s3/r3$ seems to exist. However, Fig. 9(c) shows that the behavior of $s2$ and $r2$ can be divided into three regimes, where in the final blocking regime the Avrami exponents as a function of time coincide with the ones holding for $s3$ and $r3$ within the blocking regime. So, this again shows that the scaling behavior of the different processes is a function of time and not of the fraction transformed.

Figure 10 shows results of the *s* growth mode in the three orthogonal orientations for various values of the nucleation rate [N_0=is varied between exp(57) and exp(60) $\mu m^{-3}\,s^{-1}$] in a volume of $400\times400\times400$ pixels with each a volume of $25\times25\times25$ nm^3. The other parameters were identical as for Fig. 9. These simulations in 3D space with this large total number of pixels (64 million) are very demanding particular regardingly computer memory. Principally the results obtained with $200\times200\times200$ pixels lead to the same conclusions. Again the two distinct regimes are observed with an Avrami exponent of about 3 in the JMAK regime and of about $\frac{1}{3}$ in the blocking regime, where the transition time t^* in Fig. 10(b) and the levels of the more or less straight-line segments in the Avrami plot $\{\ln[-\ln(1-x)]$ versus $\ln(t)\}$ nicely scale with the nucleation rate. In Fig. 11 t^* (defined for an Avrami exponent of 1.66) is plotted as a function of $(NG^3)^{-1/4}$. According to Eq. (8) the relation between the two should be directly proportional and this turns out to be (accurately) true. Based on the slope of the linear regression in Fig. 11 a K value in-between 2.73 and 2.75 holds. This value is slightly lower than found in the previous two sections for 2D space. With 1D growth in 2D space grains cannot grow around each other, whereas with 2D growth in 3D space this is possible and this complexity does not fully allow Eq. (8) to be equally valid for both 2D and 3D space, i.e, with a single value of K. Nevertheless the results in Figs. 10 and 11 show that overall the correspondence with Eq. (8) is still good.

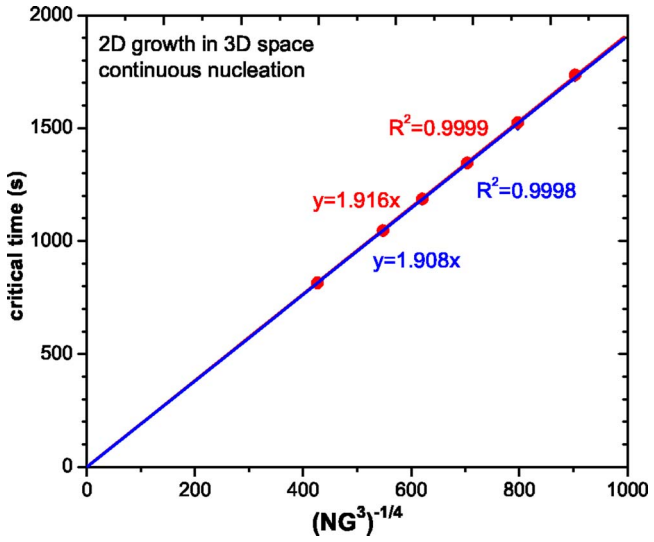

FIG. 11. (Color online) The critical time t^* as obtained from the average of 21 MC simulations versus $(NG^3)^{-1/4}$ for a constant nucleation rate and 2D *s* growth in 3D space, showing that t^* is directly proportional to $(NG^3)^{1/4}$; see Eq. (8).

D. 2D growth in 3D space of pre-existing nuclei

With pre-existing nuclei, 2D growth in 3D space within three orthogonal orientations leads to transformation kinetics where an initial JMAK regime exists characterized by an Avrami exponent with a value of exactly 2 followed by a gradual transition to a value of 0 in the blocking regime. An example of this behavior is shown in Fig. 12 for the *s*-type growth mode using parameters for the MC simulations that are given in Table I. In the same way as in Sec. IV B, where also pre-existing nuclei were considered (but for 1D growth in 2D space), the transformation stops before being complete such that the fraction transformed reaches an upper limit x_{max} below one. As predicted by Eq. (8) the extended fraction $-\ln(1-x_{max})$ is directly proportional to $(N_0)^{1/3}$, because for $t\gg t^*$: $x_{ex}=k=wK^{d_g}\sqrt[d_s]{N_0}$. Indeed, as shown in Fig. 13 this relation holds and the slope in Fig. 13 indicates a K value of 2.98 (because $w=0.05$ μm). This K value is in excellent

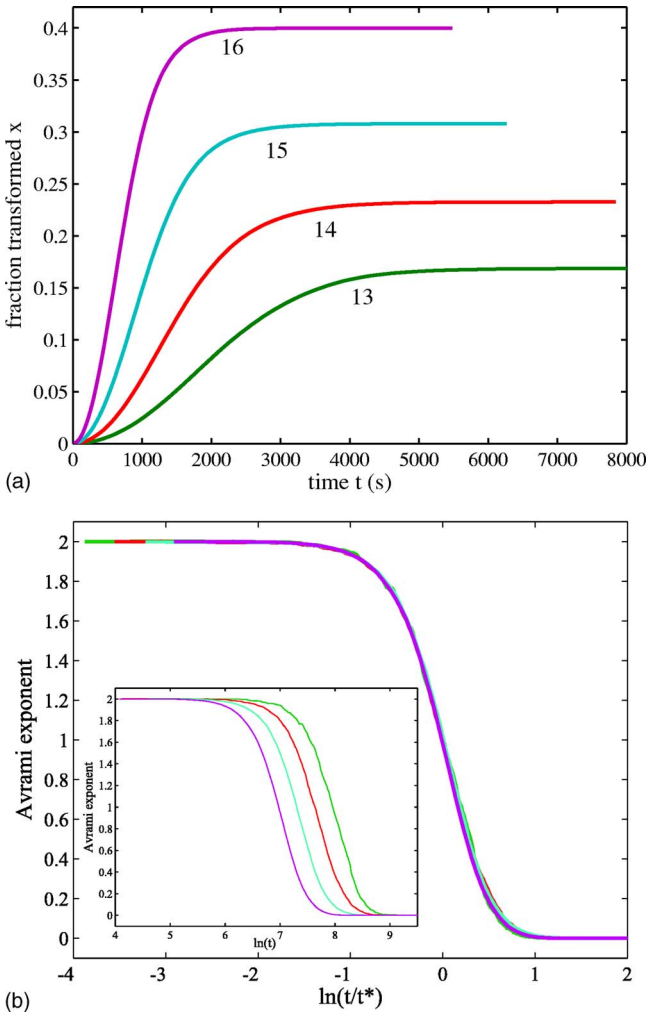

FIG. 12. (Color online) Transformation kinetics obtained from MC simulations based on pre-existing nuclei and 2D *s* growth in 3D space. The *s* grains grow with equal probability in three orthogonal orientations. The parameters used for the MC simulations are given in Table I.

agreement with the values found in Secs. IV A and IV B showing the universal validity of Eq. (8). In Sec. IV C, the two levels of the Avrami exponent in the JMAK and blocking regime as based on the MC simulations did not exactly obey the predicted values 3 and $\frac{1}{3}$, whereas in the present section the simulated two levels have exactly the values 2 and 0 as predicted by theory [Eq. (8)]. This may explain why the presently found K value is still in agreement with the values found in Secs. IV A and IV B, whereas the value found in Sec. IV C slightly deviates.

An obvious question: what is the physical origin of this universal K value? The (incomplete) answer is related to the average length (1D or 2D) grains are able to grow before blocking occurs and apparently the stochastics of the process are such that this length is K times the average mutual distance between nuclei and this average distance is $(\sqrt[d_s]{N_0})^{-1}$ with N the total number of nuclei that have developed up to the time considered (i.e., including all the phantom nuclei in cases other than pre-existing nuclei). Using this knowledge it is clear that K cannot be smaller than 1 and the probability

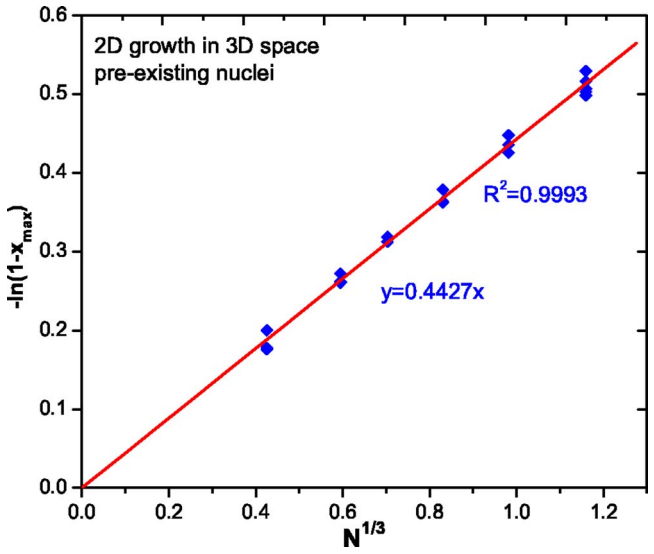

FIG. 13. (Color online) Results of MC simulations holding for pre-existing nuclei and 2D *s* growth in 3D space; grains grow with equal probability in three orthogonal orientations. The extended fraction based on the maximum attainable fraction transformed is plotted versus the cube root of the total number of pre-existing nuclei per unit of area N.

that it has a value beyond 5 is already small and strongly decreasing, because blocking should then have been occurred.

V. CONCLUSIONS

MC simulations of 1D growth in 2D space have been presented where the growth (with constant rate G) has equal probability of occurring in two or three different nonparallel orientations and where the total number of nuclei N is assumed to be a simple power of time t, i.e., $N=N_0t^a$ $(a\geqslant 0)$. Also MC simulations of 2D growth in 3D space have been presented where the grains grow with equal probability in three (two or one) orthogonal orientations in space. All these simulations show transformation kinetics that cannot be reproduced by the traditional Johnson-Mehl-Avrami-Kolmogorov (JMAK) theory, because of the hard impingement that occurs due to the anisotropic growth. However, it is shown that up to a critical time t^* always an initial regime is present where JMAK theory prevails and after this time a blocking regime is entered. The present MC simulations show that t^* is directly proportional to $\sqrt[d_{s+a}]{N_0G^{d_s}}$, with d_s the dimensionality of space. The JMAK regime is characterized by an Avrami exponent equal to d_g+a, with d_g the dimensionality of growth, and the blocking regime by an Avrami exponent equal to a/d_s. The MC simulations show that within the blocking regime the extended fraction is directly proportional to $\sqrt[d_s]{N_0}$ and independent of the growth shape and growth rate G. Analytical theory has been developed that is able to reproduce very well all the numerical results of the MC simulations on d-1 dimensional growth in d dimensional space (d is 2 or 3) and that for $t\ll t^*$ exactly reproduces JMAK theory. The existence of a universal constant K within

the theory with a value near 2.95 has been demonstrated.

Extrapolating the discrete MC simulations to continuum space indicates, for 1D growth in 2D space where growth has equal probability to occur in two orientations with mutual angle α, that (i) the extended fraction in the blocking regime is directly proportional to $(\sin\alpha)^{-1/2}$, (ii) t^* is directly proportional to $(\sin\alpha)^{-1/(2+a)}$, and (iii) the initial JMAK regime is independent of the mutual orientation of the grains.

ACKNOWLEDGMENT

Maarten Hilgenga and Patrick Onck are gratefully acknowledged for provision of computer facilities.

APPENDIX A

For 2D growth in 3D space, where 2D plates with thickness w are assumed to have equal probability to grow in three orthogonal orientations, the average length these plates are able to grow within the blocking regime is now the reciprocal of the total number of nuclei (at time t) to the power $\frac{1}{3}$ instead of $\frac{1}{2}$ in 2D space. Using this approach it is implicitly assumed that the 2D grains do not grow around each other. Their area is the square of this length and their volume is thus

$$V(t-\tau) = \frac{wC^2}{(N_0\tau^a)^{2/3}}. \tag{A1}$$

Inserting Eq. (A1) in Eq. (1b) yields

$$x_{ex} = \int_{t^*}^{t} aN_0\tau^{a-1}\frac{wC^2}{(N_0\tau^a)^{2/3}}d\tau \tag{A2a}$$

with t^* given by

$$Gt^* = \frac{C}{[N_0(t^*)^a]^{1/3}} \Rightarrow t^* = \sqrt[a+3]{\frac{C^3}{N_0G^3}}. \tag{A2b}$$

Integration of Eq. (A2a) gives

$$x_{ex} = 3wC^2[N_0(t-t^*)^a]^{1/3}, \tag{A3}$$

where up to t^* the extended fraction obeys normal JMAK behavior according to Eq. (2) and after t^* the blocking regime is entered and the total extended fraction is thus given by the sum of the fractions pertaining to the JMAK and the blocking regime:

$$x_{ex} = 3wC^2[N_0(t-t^*)^a]^{1/3} + \left(\frac{g}{1+a}\right)\left(\frac{2}{2+a}\right)N_0G^2(t^*)^{2+a}. \tag{A4}$$

*Email address: b.j.kooi@rug.nl

[1] A. N. Kolmogorov, Izv. Akad. Nauk SSSR, Ser. Mat. **3**, 355 (1937).

[2] W. A. Johnson and R. Mehl, Trans. AIME **185**, 416 (1939).

[3] M. Avrami, J. Chem. Phys. **7**, 1103 (1939); **8**, 212 (1940); **9**, 177 (1941).

[4] M. P. Shepilov and D. S. Baik, J. Non-Cryst. Solids **171**, 141 (1994).

[5] T. Pusztai and L. Granasy, Phys. Rev. B **57**, 14110 (1998).

[6] D. P. Birnie III and M. C. Weinberg, J. Chem. Phys. **103**, 3742 (1995).

[7] M. C. Weinberg and D. P. Birnie III, J. Non-Cryst. Solids **202**, 290 (1996).

[8] B. S. Lement and M. Cohen, Acta Metall. **4**, 469 (1956).

[9] M. Hillert, Acta Metall. **7**, 653 (1959).

[10] T. Tagami and S.-I. Tanaka, Acta Mater. **45**, 3341 (1997).

[11] M. J. Starink, J. Mater. Sci. **36**, 4433 (2001).

[12] V. Sessa, M. Fanfoni, and M. Tomellini, Phys. Rev. B **54**, 836 (1996).

[13] D. Crespo and T. Pradell, Phys. Rev. B **54**, 3101 (1996).

[14] R. M. Bradley and P. N. Strenski, Phys. Rev. B **40**, 8967 (1989).

[15] R. A. Ramos, P. A. Rikvold, and M. A. Novotny, Phys. Rev. B **59**, 9053 (1999).

[16] B. J. Kooi, Phys. Rev. B **70**, 224108 (2004).

[17] J. W. Christian, *The Theory of Transformations in Metals and Alloys* (Pergamon Press, Oxford, 1965).

[18] Clinton DeW. Van Siclen, Phys. Rev. B **54**, 11845 (1996).

[19] M. Tomellini and M. Fanfoni, Phys. Rev. B **55**, 14071 (1997).

[20] S. Ranganathan and M. von Heimendahl, J. Math. Phys. **16**, 2401 (1981).

[21] G. Ruitenberg, A. K. Petford-Long, and R. C. Doole, J. Appl. Phys. **92**, 3116 (2002).